Modeling of regional dynamic CO_2 reactivity in respiratory related brain areas using BOLD fMRI

G. D. Mitsis, *Member, IEEE*, A. K. Harvey, S. Dirckx, S.D. Mayhew, R. Rogers, I. Tracey, R.G. Wise and K. T. S. Pattinson

***Abstract*— The cerebrovascular bed is very sensitive to CO_2 changes, particularly the areas responsible for generation and control of respiratory rhythm. We have used BOLD functional magnetic resonance imaging (fMRI) and externally induced CO_2 challenges that stimulate respiration, to identify respiratory areas in-vivo in humans and to quantify the dynamic effects of CO_2 on the BOLD fMRI signal (dynamic CO_2 reactivity). We sought to identify regional differences in dynamic reactivity within the brainstem and other respiratory related areas (thalamus) by using linear impulse response (IR) and nonlinear Volterra models, as well as experimental measurements obtained during spontaneous breathing and larger externally induced step CO_2 changes (end-tidal forcing). The results revealed areas in the brainstem and thalamus that responded strongly to the external CO_2 stimuli, which correspond to respiratory nuclei identified in recent rodent studies, as well as pronounced regional differences in CO_2 reactivity.**

I. Introduction

The cerebral vasculature is exquisitely sensitive to arterial CO_2 variations. Spontaneous fluctuations of arterial CO_2 tension have been shown to correlate with low-frequency oscillations of both cerebral blood flow velocity, obtained by transcranial Doppler ultrasound [1], and with the blood oxygen level dependent (BOLD) signal, obtained by functional magnetic resonance imaging (fMRI) [2]. In this latter study, significant regional differences in CO_2 sensitivity were revealed throughout the brain.

Moreover, it is well known that brainstem respiratory control centers are particularly sensitive to CO_2 [3]. Recent advances in fMRI have enabled imaging of the brainstem with better resolution and accuracy, providing the opportunity to translate direct animal electrophysiological data, which are not feasible in humans, regarding respiratory rhythm generation and control [4]. Brainstem activity has been observed in previous fMRI studies of human respiration, relating to dyspnea or volitional control of breathing [5, 6].

Therefore, in this study we examined responses to spontaneous and chemically stimulated breathing in healthy human volunteers with BOLD fMRI. In order to maximize resolution, fMRI was limited to a narrow field of view focused on the brainstem. We have examined in detail the hemodynamic response to both spontaneous and larger, externally-induced CO_2 changes (dynamic CO_2 reactivity) by using linear impulse response as well as nonlinear Volterra models. We sought to compare the hemodynamic responses between the two stimulus types and to identify regional differences in dynamic CO_2 reactivity within respiratory related areas.

II. Methods

A. Experimental Methods

12 right-handed healthy volunteers, age 32 (SD(5)) yrs (3 female) participated in this study after giving written informed consent in accordance with the Oxfordshire Clinical Research Ethics Committee.

Respiratory protocols: The subjects wore a tight fitting facemask (Hans Rudolph, Kansas City, MO, USA) attached to a breathing system, which delivered mixtures of air, O_2 and CO_2. A minimum of ten minutes was allowed to adapt to the mask. Continuous recordings were made of tidal CO_2 and O_2, respiratory volume and oxygen saturations.

For the first half of the study (baseline "resting breathing" experiment) the subjects were asked to perform no particular task other than to remain awake. In the second half of the experiment, we delivered intermittent CO_2 challenges to stimulate breathing. The CO_2 challenges were delivered via a computer controlled gas mixing system (dynamic end tidal forcing) [7]. The CO_2 challenges were designed to raise the subject's $P_{ET}CO_2$ by either 2 or 4 mmHg above a baseline level and lasted between 11 and 120 seconds (Figure 1).

This methodology gave a good range of $P_{ET}CO_2$ values for comparison with the "resting-state" data from the first half of the experiment. During this part of the experiment end-tidal oxygen ($P_{ET}O_2$) was maintained at 200mmHg, independent of changes in breathing, a value that is mildly

Manuscript received July 5, 2008. This work was supported in part by the European Social Fund (75%) and National Resources (25%) - Operational Program Competitiveness - General Secretariat for Research and Development (Program ENTER 04), by the Association of Anaesthetists of Great Britain and Ireland, the International Anesthesia Research Society and by the Medical Research Council (UK).

G.D. Mitsis was with the Centre for Functional Magnetic Resonance Imaging of the Brain (FMRIB), University of Oxford, Oxford, United Kingdom. He is now with the Institute of Communication and Computer Systems, National Technical University of Athens, Greece (phone: +30-210-7722466; fax: +30-210-7721076; email: gmitsis@esd.ntua.gr).

A.K. Harvey, S. Dirckx, S.D. Mayhew and K.T.S. Pattinson are with the Centre for Functional Magnetic Resonance Imaging of the Brain (FMRIB), University of Oxford, Oxford, United Kingdom.

R. Rogers is with the Nuffield Department of Anaesthetics, University of Oxford, Oxford, United Kingdom.

I. Tracey is with the Centre for Functional Magnetic Resonance Imaging of the Brain (FMRIB) and with the Department of Human Anatomy and Genetics, University of Oxford, Oxford, United Kingdom.

R.G. Wise was with the Centre for Functional Magnetic Resonance Imaging of the Brain (FMRIB), University of Oxford, Oxford, United Kingdom. He is now with CUBRIC, School of Psychology, Cardiff University, Cardiff, United Kingdom.

above normal.

BOLD imaging: Two thousand seven hundred T2* weighted echo planar image (EPI) volumes were acquired on a Siemens Trio 3T scanner. The field of view (light gray shadow - Figure 2) comprised 16 coronal oblique slices of the brainstem (sequence parameters: TE=30 ms, TR=1 s, voxel size 2.5x2.5x3mm, flip angle 70°). The experiment was divided into two stages, although scanning was continuous: The first 1130 images (18 minutes 50 seconds) comprised the baseline experiment and the final 1530 images (25 minutes 30 seconds) comprised the CO_2 stimulation experiment. The duration was determined by adaptation of a similar CO_2 challenge protocol [8] for use in the MRI scanner. We also acquired a single volume whole head echo planar image taken with the same resolution and orientation as the brainstem scans to aid with registration to each subjects' structural MRI scan and a high resolution T1 weighted structural scan (voxel size 1x1x1mm) to aid registration to common stereotactic space.

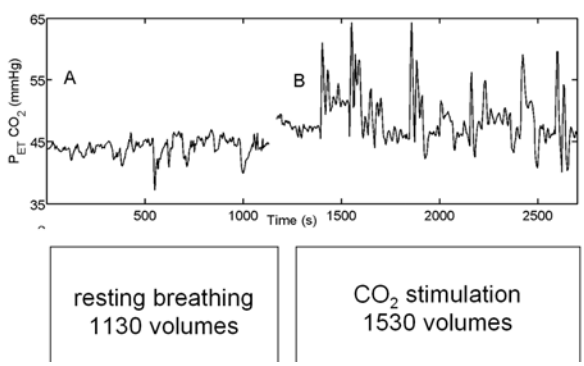

Fig. 1. Experimental protocol. The normal breathing protocol preceded the externally-induced CO_2 stimulation protocol (end-tidal forcing).

B. Mathematical Methods

Image preprocessing was carried out by using the Oxford Centre for Functional Magnetic Resonance Imaging of the Brain Software Library (FMRIB, Oxford, UK, FSL version 4.0). The following prestatistics processing were applied: removal of non brain structures (i.e. skull and surrounding tissues), spatial smoothing by using a Gaussian kernel of 5mm FWHM, mean-based intensity normalization of all volumes by the same factor, and high pass temporal filtering.

The brainstem is particularly susceptible to respiratory and cardiac noise. Therefore, in addition to standard motion correction techniques, we also employed a modified version of a noise correction technique, RETROICOR [9], in order to correct for cardiac and respiratory related noise. After preprocessing, the functional scans were registered to the MNI152 standard space using a linear registration method (FLIRT [10]). Registration of the functional images to the T1 structural images was specifically optimized for the brainstem by using weighting masks that ensured accurate brainstem alignment.

Time-series statistical analysis was carried out using FILM with local autocorrelation correction [11]. For the first level analysis we used a general linear model where the regressor of interest was $P_{ET}CO_2$. We assumed a 6 second hemodynamic delay but included the temporal derivative of the CO_2 regressor to account for variation around this value. Voxel-wise statistical analysis was extended to a second (group) level in a mixed effects analysis. Z statistical images were thresholded using clusters determined by Z>2.3 and a (corrected) cluster significance threshold of P=0.05. We assessed the responsiveness of BOLD signal to hypercapnia, defined as the BOLD signal change per unit change in $P_{ET}CO_2$. Paired t-tests were performed within FEAT (http://www.fmrib.ox.ac.uk/fsl/) to compare the CO_2 response between those derived from the spontaneous "resting state" fluctuations in $P_{ET}CO_2$ and those derived from CO_2 challenges, by contrasting the mean and difference of the first level analyses. We were particularly interested in identifying brain regions which demonstrated the strongest increase in BOLD CO_2 sensitivity during external CO_2 administration.

In order to further characterize the nature of the BOLD responses and examine the characteristics of dynamic CO_2 reactivity, we performed a post-hoc region of interest (ROI) analysis. For this reason, anatomical ROIs were drawn in standard space, corresponding to anatomical areas in the area scanned (pons, medulla, thalamus, and putamen). Moreover, functional ROIs were defined from the activations seen in the contrast BOLD images using a threshold of Z > 2.9 and comprised the following areas: rostral dorsal pons (Kölliker-Fuse / parabrachial nucleus), inferior pons nuclei (ventral respiratory group), the left ventral posterior lateral nucleus of the thalamus and the left ventrolateral and bilateral ventroanterior nuclei of the thalamus.

Dynamic CO_2 reactivity was assessed by using linear (impulse response) and nonlinear (Volterra) models to quantify the relationship between $P_{ET}CO_2$ and the averaged BOLD signal within each anatomically or functionally defined ROI. In this context, we employed the general Volterra model, which is given below for a Q-th order nonlinear system:

$$\begin{aligned} y(n) &= \sum_{q=0}^{Q} \sum_{m_1} \ldots \sum_{m_2} k_q(m_1,\ldots,m_q) x(n-m_1)\ldots x(n-m_q) = \\ &k_0 + \sum_{m} k_1(m) x(n-m_1) + \\ &+ \sum_{m_1}\sum_{m_2} k_2(m_1,m_2) x(n-m_1) x(n-m_2) + \ldots \end{aligned} \tag{1}$$

where $x(n)$ and $y(n)$ are the system input and output respectively (i.e., $P_{ET}CO_2$ and BOLD signal) and $k_q(m_1,\ldots,m_q)$ are the Volterra kernels of the system, which describe the linear (q=1) and nonlinear (q>1) dynamic effects of the input on the output. The model of (1) reduces to the convolution sum for a linear system (Q=1), with $k_1(m)$ corresponding to the impulse response of the system. This approach, termed the Volterra-Wiener approach, has been

employed extensively for modeling physiological systems, since it is well-suited to their complexity [12].

The impulse response or Volterra kernels can be estimated efficiently from input-output data, by utilizing functional expansions in terms of the orthonormal Laguerre basis [12]:

$$k_q(m_1,...,m_q) = \sum_{j_1=0}^{L} ... \sum_{j_q=j_{q-1}}^{L} c_{j_1...j_q} b_{j_1}(m_1)...b_{j_1}(m_q) \qquad (2)$$

where c_j are the expansion coefficients, $b_j(m)$ is the j-th order Laguerre function and L+1 is the total number of functions that yields an adequate system representation. By combining (1), (2) in matrix form:

$$\mathbf{y}=\mathbf{V}\mathbf{c}+\boldsymbol{\varepsilon} \qquad (3)$$

where the n-th row of $\mathbf{V}$ is given by [1, $v_1(n)$, …, v_L(n), $(v_1(n))^2$, $v_1(n)\cdot v_2(n)$,…, $v_1(n)\cdot v_L(n)$, $(v_2(n))^2$, $v_2(n)\cdot v_3(n)$, …, $(v_L(n))^2$] for a second-order system (Q=2) with $v_j(n)$ denoting the convolution of the input with the j-th order Laguerre function. The expansion coefficients are then obtained by the least-squares solution of (3):

$$\mathbf{c}_{\mathbf{est}}=[\mathbf{V}^{\mathbf{T}}\mathbf{V}]^{-1}\mathbf{V}^{\mathbf{T}}\mathbf{y} \qquad (4)$$

Model performance was assessed by the normalized mean-square error (NMSE) of the output prediction, which is defined as the mean-squared model residuals divided by the corresponding mean-squared true BOLD signal output.

III. Results

The main effect of the CO_2 challenges on breathing was to increase minute ventilation from (mean (±SD)) 5.4 (±1.5) l.min^{-1} during quiet breathing to 9.6 (±3.4) l.min^{-1} P<0.01), while mean $P_{ET}CO_2$ rose from 44.4 (±1.1) mmHg to 47.7 (±2.0) mmHg (P<0.01). End tidal oxygen levels were 105 (±4) mmHg during quiet respiration and 209 (±1) mmHg during the CO_2 challenges (P<0.001).

By comparing the signal changes from the CO_2 challenges with those correlated with the natural resting-state fluctuations in CO_2 we identified brain areas that demonstrated an increase in BOLD sensitivity to CO_2. The areas with this stronger response during external CO_2 challenges were as follows: bilaterally in the anteroventral (AV) thalamus and in the ventral posterior lateral (VPL) nucleus of the thalamus, the left ventrolateral (VL) nucleus of the thalamus, and in the midline in the rostral dorsal pons, the inferior ventral pons, and in the dorsal and ventrolateral medulla.

The brain areas with a stronger BOLD sensitivity to CO_2 stimulation compared to "resting-state" spontaneous fluctuations in $P_{ET}CO_2$ are shown in Fig. 2. The area scanned is shown in lighter grey scale, and superimposed on the subjects' mean high resolution image transformed to MNI standard space (darker grey). The functional ROIs used to subsequently calculate dynamic CO_2 reactivity were based on this group map, while the anatomical ROIs were hand-drawn in MNI space.

Nonlinear models (Q=2 in Eq. (1)) reduced the prediction NMSE marginally for most (7 out of 12) subjects during forcing conditions, implying a linear CO_2-BOLD relation, while the reduction was relatively larger during resting conditions (Table I). Note that the NMSEs obtained during resting conditions were considerably higher due to the reduced signal-to-noise ratio. Therefore, we present results obtained from linear models, whereby dynamic CO_2 reactivity is described by the system impulse response function. Representative model predictions achieved by linear and nonlinear models for one functional ROI (AV thalamus) are shown in Fig. 3, where it can be seen that $P_{ET}CO_2$ changes are clearly correlated with low-frequency BOLD oscillations both during baseline (resting) and end-tidal forcing conditions.

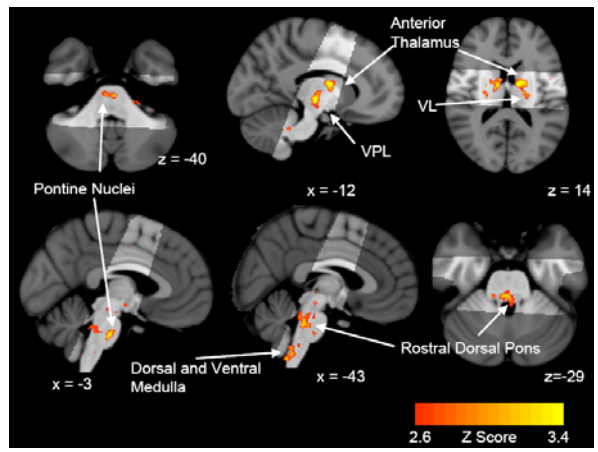

Fig. 2. Group map of brain areas with a stronger BOLD sensitivity to CO_2 stimulation compared to spontaneous fluctuations in $P_{ET}CO_2$ in MNI space. Significant regions are displayed with a threshold of Z>2.6, with a cluster probability threshold of P<0.05. Abbreviations: AV anteroventral nucleus of thalamus, VPL ventral posterior lateral nucleus of the thalamus, VL ventrolateral nucleus of thalamus.

TABLE I
NORMALIZED MEAN SQUARE ERRORS (NMSE) FOR LINEAR AND NONLINEAR MODELS OF DYNAMIC CO_2 REACTIVITY

BRAIN REGION	NMSE (SE) [%]			
	Forcing		Resting	
	Linear	Nonlinear	Linear	Nonlinear
Medulla	67.9(3.7)	66.1(3.4)	94.0(2.6)	91.5(3.0)
Pons	51.8(2.7)	49.3(1.9)	91.5(2.3)	88.6(2.5)
Thalamus	45.6(4.6)	41.6(3.1)	86.8(3.7)	82.6(4.0)
AV Thalamus	48.8(4.1)	45.7(3.3)	91.7(2.2)	88.6(2.6)
VL Thalamus	61.8(3.2)	58.8(2.6)	95.7(1.1)	93.9(1.2)
Rostral dorsal pons (KF/PB)	76.9(3.5)	74.8(3.5)	97.9(0.6)	96.7(0.6)
Pontine nuclei (VRG)	60.0(4.1)	58.0(3.8)	94.4(1.5)	91.5(2.1)

KF/PB: Kolliker Fuse/parabrachial nuclei
VRG: Ventral respiratory group

The dynamic CO_2 reactivity waveforms for different anatomically and functionally defined regions, averaged over all subjects, are shown in Figure 4 during spontaneous and forcing conditions. Significant regional variability can be observed, with the functionally defined areas (e.g., AV Thalamus) exhibiting increased sensitivity compared to the anatomically defined (larger) ROIs. These waveforms quantify the dynamic effects of CO_2 on the BOLD signal, suggesting that a CO_2 increase will result in a BOLD increase, with the maximum instantaneous effect occurring

after around 4-8 sec (depending on the region and stimulus type). While the initial part of the waveforms suggest a similar dynamic response to spontaneous and larger CO_2 changes (though the response to the latter is faster), the waveform obtained during resting conditions exhibited a late undershoot, that is absent from the forcing waveforms.

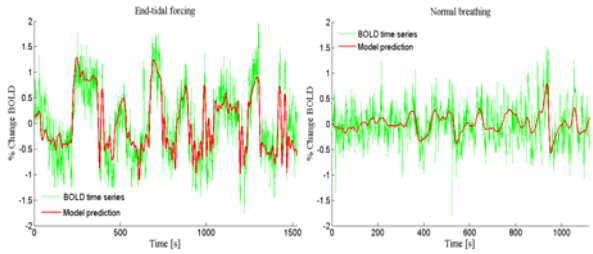

Fig. 3. Representative linear and nonlinear model predictions for the AV Thalamus functional ROI (Fig. 2) during resting (left panel) and end-tidal forcing (right panel). Note that $P_{ET}CO_2$ changes explain a considerable fraction of slow BOLD signal variations both during resting and forcing conditions.

The differential response characteristics to the two stimulus types for specific brain regions is further illustrated in Fig. 5, where we show the averaged dynamic CO_2 reactivity waveform (solid line: mean, dashed lines: standard error) in the AV thalamus (top panel) and pontine nuclei (bottom panel). While the former exhibits a significantly stronger response to the CO_2 challenges, with a significantly larger peak value and a shorter time-to-peak, the latter is equally sensitive to the two types of stimuli.

IV. Discussion and Conclusions

In this study, we have examined the hemodynamic response to CO_2 (dynamic CO_2 reactivity) in brain regions that are implicated in respiratory control by utilizing BOLD fMRI. Imaging studies of the respiratory system are challenging because changes in arterial CO_2 levels cause confounding effects on the BOLD signal. We compared the responses to externally-induced CO_2 challenges to resting breathing to dissociate the vasodilatory effects of CO_2 from its neuronal, respiratory stimulant effects caused by the larger CO_2 challenges, as we hypothesized that neural activation due to the latter would elicit an additional contribution to the BOLD response. These stronger responses were both reflected on the resulting contrast images (Fig. 2), as well as on the characteristics of the hemodynamic response, which exhibited higher peak values and faster rise times in particular brain regions (Figs. 4 and 5).

The main findings in the brainstem were signal increases in the rostral dorsal pons, the inferior ventral pons and the dorsal and ventral medulla (Fig. 2). The activation in dorsal rostral pons is possibly analogous to activity in the Kolliker-Fuse and parabrachial (KF/PB) nuclei, which has been defined recently in humans [13] and which has been studied in rats regarding its role in respiratory control.

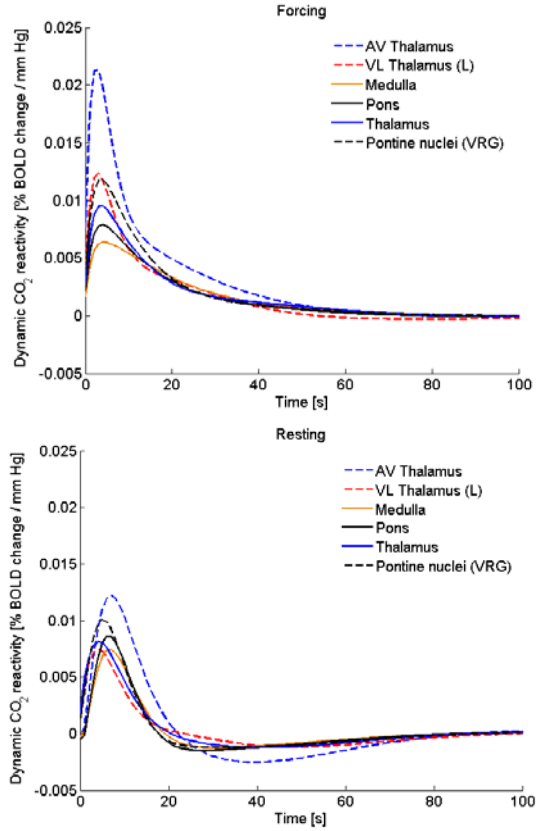

Figure 4. Dynamic CO_2 reactivity of anatomical and functional ROIs during forcing (top panel) and resting (bottom panel) conditions. The regional variability of CO_2 reactivity is evident, while its waveform was different between the two stimulus types, with the undershoot observed during normal breathing being absent during forcing conditions. AV: anteroventral VL: ventrolateral, VRG: Ventral Respiratory Group. Solid lines correspond to anatomically defined ROIs and dashed lines correspond to functionally defined ROIs.

Activity in this region of the dorsal rostral pons has been identified in two human fMRI studies of inspiratory loading [14], and breath holding [15]. We suggest that the activity demonstrated in the dorsal rostral pons in the present study represents both direct local stimulation of chemoreceptors and also afferents inputs from the lower brainstem including the ventral lateral medulla and the dorsal medulla.

The exact location of the ventral respiratory group (VRG) has not yet been confirmed in humans, but is likely to be located in the upper medulla and the lower pons. We also observed activation in the ventrolateral medulla and in the dorsal medulla (Fig. 2). These areas correspond with known locations of chemoreceptive and integrative sites for respiration. In rodent studies the pre-Bötzinger complex has been identified as an important rhythmogenic and chemosensitive nucleus in the ventral lateral medulla [4], although it has not formally been identified in humans. The unilateral activations observed in the medulla may relate to technical aspects of imaging the lower brainstem.

The activity in the AV thalamic nucleus implicates its role in mediating sensory and affective components of respiration and has been observed in two previous studies

[6, 15]. We also observed signal increases in the left VL, the left VPL nuclei of the thalamus in agreement with [15, 16]. Moreover, thalamic activity is supported by direct recordings in animals studies that implicate it as an important relay for respiratory sensations [17].

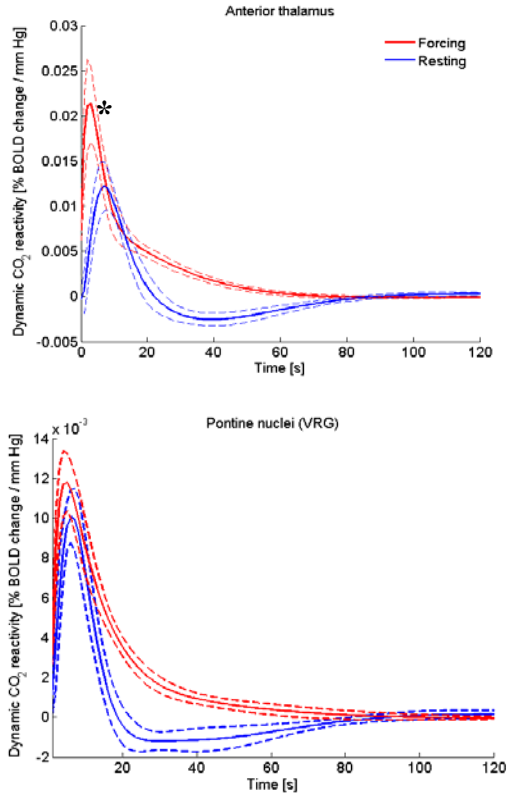

Figure 5. Examples of differential hemodynamic responses to the two stimulus types. The AV thalamus reactivity curve during forcing conditions exhibited larger peak values and faster characteristics, while in other activated areas (Fig. 2), such as the pontine nuclei, differences were less pronounced. * P<0.05 increase in peak value compared to resting.

While the voxel-wise maps of Fig. 2 are based on the magnitude of the regression coefficients with respect to the $P_{ET}CO_2$ regressor in the employed general linear model, examination of the hemodynamic response to the CO_2 changes (Figs. 4-5) provides additional information regarding the precise dynamic effects of CO_2 on the BOLD signal. The reactivity waveforms generally agree with previously reported models of the dynamic effects of CO_2 on cerebral blood flow velocity in the middle cerebral artery [1]. The results revealed considerable regional differences in the form of the hemodynamic response (Fig. 4), which, as expected, reflect the results of Fig. 2, i.e., the functionally defined ROIs exhibited waveforms with larger peak values and faster rise times. However, we also observed differences between functionally defined regions (Fig. 5), with the AV Thalamus exhibiting dynamic reactivity during forcing conditions with significantly increased peak values and faster rise times. These observations may provide additional evidence regarding the precise response characteristics of the respiratory areas to chemical stimuli and further dissociation of vascular from neural responses. They also suggest that using regionally specific hemodynamic responses in the general linear model may improve the statistical sensitivity of voxel-wise analyses in similar studies. Finally, the lack of a late undershoot in the forcing CO_2 reactivity curves may reflect a stronger response of the central chemoreceptors to the larger, externally-induced CO_2 challenges.

References

[1] G. D. Mitsis, M. J. Poulin, P. A. Robbins, and V. Z. Marmarelis, "Nonlinear modeling of the dynamic effects of arterial pressure and CO_2 variations on cerebral blood flow in healthy humans," *IEEE Trans. Biomed. Eng.,* vol. 51, pp. 1932-1943, 2004.

[2] R. G. Wise, K. Ide, M. J. Poulin, and I. Tracey, "Resting fluctuations in arterial carbon dioxide induce significant low frequency variations in BOLD signal," *Neuroimage,* vol. 21, pp. 1652-64, Apr 2004.

[3] J. L. Feldman, G. S. Mitchell, and E. E. Nattie, "Breathing: rhythmicity, plasticity, chemosensitivity," *Annu Rev Neurosci,* vol. 26, pp. 239-66, 2003.

[4] J. L. Feldman and C. A. Del Negro, "Looking for inspiration: new perspectives on respiratory rhythm," *Nat Rev Neurosci,* vol. 7, pp. 232-42, Mar 2006.

[5] D. R. Corfield, G. R. Fink, S. C. Ramsay, K. Murphy, H. R. Harty, J. D. Watson, L. Adams, R. S. Frackowiak, and A. Guz, "Evidence for limbic system activation during CO2-stimulated breathing in man," *J Physiol,* vol. 488 (Pt 1), pp. 77-84, Oct 1 1995.

[6] L. C. McKay, K. C. Evans, R. S. Frackowiak, and D. R. Corfield, "Neural correlates of voluntary breathing in humans," *J Appl Physiol,* vol. 95, pp. 1170-8, Sep 2003.

[7] P. A. Robbins, G. D. Swanson, and M. G. Howson, "A prediction-correction scheme for forcing alveolar gases along certain time courses," *J Appl Physiol,* vol. 52, pp. 1353-7, May 1982.

[8] M. E. Pedersen, M. Fatemian, and P. A. Robbins, "Identification of fast and slow ventilatory responses to carbon dioxide under hypoxic and hyperoxic conditions in humans," *J Physiol,* vol. 521 Pt 1, pp. 273-87, Nov 15 1999.

[9] G. H. Glover, T. Q. Li, and D. Ress, "Image-based method for retrospective correction of physiological motion effects in fMRI: RETROICOR," *Magn Reson Med,* vol. 44, pp. 162-7, Jul 2000.

[10] M. Jenkinson, P. Bannister, M. Brady, and S. Smith, "Improved optimization for the robust and accurate linear registration and motion correction of brain images," *Neuroimage,* vol. 17, pp. 825-41, Oct 2002.

[11] M. W. Woolrich, B. D. Ripley, M. Brady, and S. M. Smith, "Temporal autocorrelation in univariate linear modeling of FMRI data," *Neuroimage,* vol. 14, pp. 1370-86, Dec 2001.

[12] V. Marmarelis, *Nonlinear Dynamic Modeling of Physiological Systems*. Piscataway, NJ: IEEE-Wiley, 2004.

[13] A. M. Lavezzi, G. Ottaviani, L. Rossi, and L. Matturri, "Cytoarchitectural organization of the parabrachial/kolliker-fuse complex in man," *Brain Dev,* vol. 26, pp. 316-320, 2004.

[14] D. Gozal, O. Omidvar, K. A. Kirlew, G. M. Hathout, R. Hamilton, R. B. Lufkin, and R. M. Harper, "Identification of human brain regions underlying responses to resistive inspiratory loading with functional magnetic resonance imaging," *Proc Natl Acad Sci U S A,* vol. 92, pp. 6607-11, Jul 3 1995.

[15] L. C. McKay, L. Adams, R. S. J. Frackowiak, and D. R. Corfield, "A bilateral cortico-bulbar network associated with breath holding in humans, determined by functional magnetic resonance imaging," *Neuroimage,* vol. 40, pp. 1824-1832, 2008.

[16] K. C. Evans, R. B. Banzett, L. Adams, L. McKay, R. S. Frackowiak, and D. R. Corfield, "BOLD fMRI identifies limbic, paralimbic, and cerebellar activation during air hunger," *J Neurophysiol,* vol. 88, pp. 1500-11, Sep 2002.

[17] Z. Chen, F. L. Eldridge, and P. G. Wagner, "Respiratory-associated rhythmic firing of midbrain neurones in cats: relation to level of respiratory drive," *J Physiol,* vol. 437, pp. 305-325, 1991.